A R C H I V E S O F M E T A L L U R G Y A N D M A T E R I A L S
Volume 58 2013 Issue 2
DOI: 10.2478/amm-2013-0002

J. BIDULSKÁ*, T. KVAČKAJ*, I. POKORNÝ*, R. BIDULSKÝ*, M. ACTIS GRANDE**

IDENTIFICATION OF THE CRITICAL PORE SIZES IN SINTERED AND ECAPed ALUMINIUM 6XXX ALLOY

PRZEWIDYWANIE POWSTAWANIA POROWATOŚCI PODCZAS WYCISKANIA W KANALE KĄTOWYM STOPU ALUMINIUM OTRZYMANEGO METODĄ PROSZKOWĄ

The main aim of this paper is to investigate, by means of comparison of experimental studies and mathematical models, the evolution of porosity as consequence of pressing, sintering and ECAPping an aluminium based powder (6xxx). After applying the compacting pressure, specimens were dewaxed in a ventilated furnace at 400°C for 60 min. Sintering was carried out in a vacuum furnace at 610°C for 30 min. The specimens were then ECAPed for 1 pass. The 2-dimensional quantitative image analysis was carried out by means of SEM and OM for the evaluation of the aforementioned characteristics. Results show the effect of processing parameters on the fracture/microstructure behaviour of the studied aluminium PM alloy. Quantitative image analysis, as well as fractographic interpretation and microstructure identification of weak sites in the studied aluminium PM alloy, provide a reliable and reproducible statistical procedure for the identification of the critical pore sizes.

Keywords: aluminium alloy, ECAP, porosity, critical pore sizes, microstructure, fracture

Głównym celem pracy jest badanie zmian porowatości podczas prasowania, spiekania i wyciskania przez kanał kątowy proszku na bazie aluminium (Ai-Mg-Si-Cu-Fe) za pomocą eksperymentu i symulacji numerycznych. Po przyłożeniu ciśnienia podczas zagęszczania usuwano lepiszcze z próbek w piecu w temperaturze 400°C przez 60 minut. Spiekanie prowadzono w piecu próżniowym w temperaturze 610°C przez 30 min. Próbki następnie były wyciskane przez kanał kątowy w jednym przejściu. Dwuwymiarową ilościową analizę obrazu przeprowadzono za pomocą skaningowej mikroskopii elektronowej i mikroskopii optycznej w celu oceny wyżej wymienionych właściwości. Wyniki opisują wpływ parametrów procesu na pękanie/mikrostrukturę badanego proszku stopu aluminium. Ilościowa analiza obrazu, jak również mikrostruktury w badanym stopie proszku aluminium zapewniają wiarygodne i statystycznie powtarzalne procedury dla identyfikacji miejsc inicjacji pękania.

1. Introduction

Powder Metallurgy (PM) represents a (relatively) innovative application for the manufacturing of components with increased performances and improved tolerances. A challenge for PM, mainly in the aluminium industry, is however to compete with other technologies. Among them, severe plastic deformation (SPD) shows several potentionalities, mainly dealing with wrought aluminium alloys. Some procedures are rather popular in the SPD processing of wrought aluminium alloys, such as high-pressure torsion (HPT), equal channel angular rolling (ECAR) and equal channel angular pressing (ECAP).

High-pressure torsion (HPT) produces specimens in the form of a thin disk which is subject to a very high pressure and concurrent torsional straining. Several results suggest that HPT should be a very valuable processing tool [1-3]. On the other hand, the main disadvantage of this technique is that very small samples can be obtained and the determination of the precise strain is difficult as well.

During the ECAR processing, samples are being carried through the groove of working rollers. The process uses friction between rollers to push the sample through a die. The effect of ECAR on the structure and on the material properties has been examined in few studies [4, 5], whereas it is possible to find works related to the numerical and mathematical simulation [6, 7].

In ECAP [8], a sample, in the form of a bar or rod, is machined to fit within a channel inside a die, where the channel is machined so that it bends through a sharp angle within the die where this angle is generally equal to, or very close to, 90°. In addition [9] it has many unique features such as large strains, high strain rates, no change of shapes, and minimal load requirements.

Processing an alloy by ECAP in the absence of ageing leads to high strength but negligible uniform strain and no significant strain hardening, whereas processing by ECAP followed by ageing gives also high strength, a region of uniform strain and an overall ductility which is comparable to, and even slightly exceeds, the ductility in the solution-treated and aged condition [8-11].

Single and multiple ECAP passes have been used to process aluminium alloys [12-20]. It is important to note that

* DEPARTMENT OF METALS FORMING, FACULTY OF METALLURGY, TECHNICAL UNIVERSITY OF KOŠICE, SLOVAKIA
** POLITECNICO DI TORINO, DEPARTMENT OF APPLIED SCIENCE AND TECHNOLOGY, ALESSANDRIA, ITALY

more than 70% of the enhancement in strength levels and hardness values are achieved in aluminum alloys after a single ECAP pass [20]. Moreover, the optimum strength and microstructures are achieved the most readily when a high strain is imposed in a single processing operation rather than by introducing the same cumulative strain through several small strain increments [21]. However, in terms of PM, the presence of porosity after ECAP remains a common problem, significantly influencing the quality and the mechanical properties of the specimens. Only few authors have deepened this field of research [22-25].

2. Experimental conditions

A commercial ready-to-press aluminium based powders (ECKA Alumix 321) was used as material to be investigated. The formulation of the tested alloy is presented in Table 1 (wt. %).

TABLE 1
Chemical composition of the studied material

Al	lubricant	Mg	Si	Cu	Fe
balance	1.50	0.95	0.49	0.21	0.07

Specimens were obtained using a 2000 kN hydraulic press, applying different pressures. Unnotched impact energy specimens 55×10×10 mm^3 (ISO 5754) were prepared at two different pressing pressures 400 and 600 MPa. The green compacts were weighed with an accuracy of ±0.001 g. The dimensions were measured with a micrometer calliper (±0.01 mm). Specimens were dewaxed in a ventilated furnace (Nabertherm) at 400°C for 60 min. Sintering was carried out in a vacuum furnace (TAV) at 610°C for 30 min, with an applied cooling rate of 6°C/s.

The ECAP was realized by hydraulic equipment at room temperature, which makes it possible to produce the maximum force of 1 MN. The die channel angle was 90° and channels of diameter 10 mm in the cross section. The specimens were ECAPed for 1 pass.

The samples for microstructure evaluation were taken from locations in the centre of specimen along the length. The microstructural characterization was carried out on unetched specimens using an optical microscope LEICA MPEF4 equipped with an image analyzer and SEM Jeol 7000F. Characterization was carried out at 100× on the minimum 5 different image fields for specimens prepared by press-and-sinter and 500× for ECAPed specimens; this way, pores were recorded and processed by Leica Qwin image analysis system. Quantitative image analysis of investigated material treats pores as isolated plane two-dimensional objects in solid surroundings. In order to describe the dimensional and morphological porosity characteristics, the dimensional characteristic D_{circle} (representing the diameter of the equivalent circle showing the same area as the metallographic cross-section of the pore) and aspect ratio A (representing the ratio between major axis and minor axis of ellipse equivalent to pore; according to [26], the aspect ratio considers the stress and strain situation in the workpiece during ECAP) as well as the morphological characteristics f_{shape} and f_{circle} were processed. The description of the parameters is reported in [27, 28]. From the fracture mechanical point of view, the size and the internal notch effect of the pores must be decisive for the material performance. It comes to this that the small nanopores are rounder and their lower notch effect is less harmful for the mechanical behaviour. Considering this statement, only pores large up to 1 μm were investigated, given their potential acting as fracture initiation sites. For this reason all smaller pores were excluded from further investigation.

Equation (1) was used for evaluating the total porosity of the studied material:

$$P = \left(1 - \frac{\rho_g}{\rho_t}\right) \cdot 100 \quad [\%] \tag{1}$$

where

P – total porosity,

ρ_g – green density [g·cm^{-3}],

ρ_t – theoretical density [g·cm^{-3}].

The density of the green compacts was determined from weight and dimensional measurements, which were accurate as ±0.001 g and ±0.001 mm, respectively. The apparent density was calculated determinate using Hall apparatus according to standard MPIF 04. Theoretical density of compact was calculated according to equation (2):

$$\rho_t = \frac{100}{\sum_{i=1}^{n} \frac{w_i}{\rho_i}} \quad \left[g \cdot cm^{-3}\right] \tag{2}$$

where

w_i – the weight percentages of elements and additives,

ρ_i – the specific weight of elements and additives.

The method of least squares was used for fitting a function to a set of microstructural characterization points from experimental data by Matlab.

3. Results

The unetched microstructures of the studied aluminium alloy are presented in Fig. 1 to Fig. 3.

Fig. 1a (400 MPa) and Fig. 1b (600 MPa) show the OM microstructure of the pressed and sintered aluminium alloy. Fig. 2a, b to Fig. 3a, b show the microstructures obtained by OM and SEM, of specimens after a single ECAP pass. It can be seen that the specimens, in this case, show a more refined and elongated grain structure compared to the pressed-and-sintered specimens. A relatively high presence of pores (mix of primary, secondary and residual porosity [25]), as well as an excessive amount of residual porosity at grain boundaries, were observed after sintering. ECAP can be sufficient to achieve a good densification. The presence of adsorbed and absorbed gases by the aluminium particles, as well as water vapour present during sintering, would increase the size of the compacts and therefore reduce the sintered density, due to the volume expansion. As it has been reported in [24, 29], FEM analyses of samples after ECAP show that the porosity is located in particular in the bottom region of the workpiece, close to the outer corner of the die. The interaction of severe shear and surface oxides, which are unbreakable both during

pressing and sintering and in the following severe plastic deformation, is therefore present in the component.

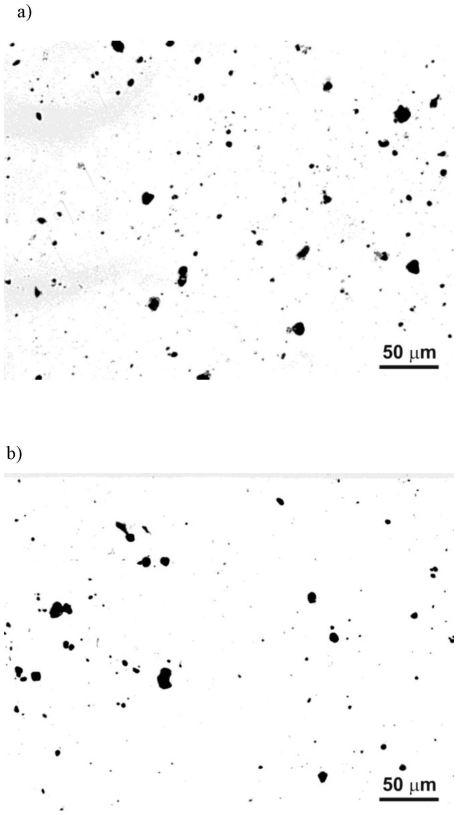

Fig. 1. a) The microstructure of studied aluminium alloy, pressed at 400 MPa and sintered; b) The microstructure of studied aluminium alloy, pressed at 600 MPa and sintered

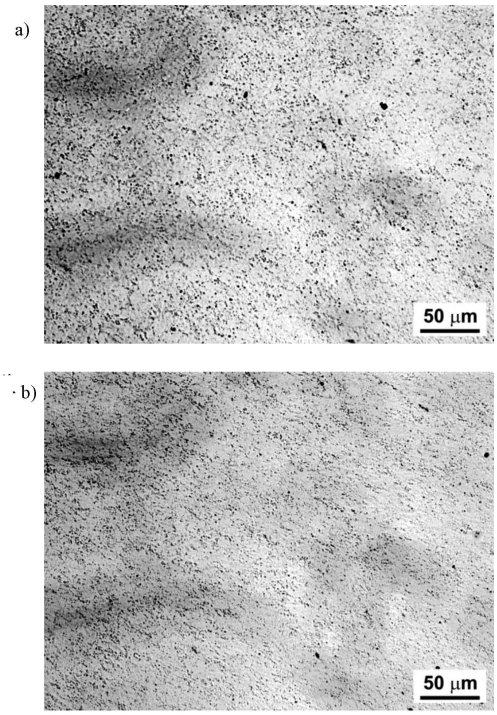

Fig. 2. a) The microstructure of studied aluminium alloy, pressed at 400 MPa, sintered and ECAPed, OM; b) The microstructure of studied aluminium alloy, pressed at 600 MPa, sintered and ECAPed, OM

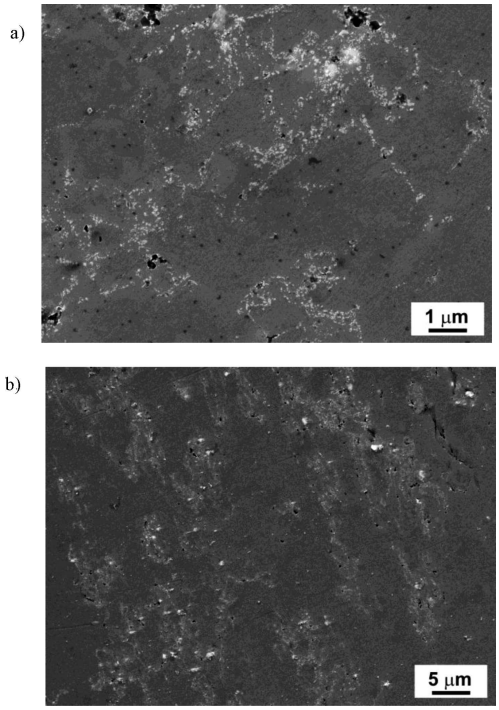

Fig. 3. a) The microstructure of studied aluminium alloy, pressed at 400 MPa, sintered and ECAPed, SEM; b) The microstructure of studied aluminium alloy, pressed at 600 MPa, sintered and ECAPed, SEM

TABLE 2

The porosity behaviour of the studied material

Applied pressing pressure	**Process state**									
	Before ECAP					**After ECAP**				
	D_{circle}	f_{shape}	f_{circle}	A	P	D_{circle}	f_{shape}	f_{circle}	A	P
[MPa]	[μm]	[-]	[-]	[-]	[%]	[μm]	[-]	[-]	[-]	[%]
400	30.64	0.70	0.92	2.24	7.88	0.97	0.67	0.91	1.88	1.69
600	23.64	0.69	0.92	2.21	7.18	0.85	0.67	0.91	1.82	1.36

Table 2 shows that the decrease of parameter D_{circle} in both pressure conditions is consistent. It is well-known that ECAP decreases the porosity content due to SPD condition and it is also able to align particles. The parameter A decreases too for both conditions from 2.24 to 1.88 and from 2.21 to 1.82, in case of pressing at 400 MPa and at 600 MPa respectively.

4. Discussion

The high levels of both compressive and tensile stresses produced in specimen during the ECAP process, combined with the high localized shear strains, may be sufficient to promote high rates of pore reduction/elimination and pore/void nucleation. The applied mean stress, known as the hydrostatic stress, induces new plasticity-driven densification mechanisms, as well as a stress-assisted diffusion mechanism [30, 31]. The grain refinement during ECAP is due to increase in the density of triple junctions that can act as preferred sites for

nanopores/voids nucleation (strain-induced porosity) [21, 25]. ECAP creates a structure characterized by some nanoporosity occurring in the areas of triple junctions. Such pores are different from those typical of PM materials (micropores), which are deriving from the compaction and/or the sintering steps. In case of ECAP, nanopores are formed during severe deformation.

Through the proposition of a so called "safety line" [26], the effect of pores as a potential fracture initiation sites (with respect to the mechanical viewpoint) was taken into account and analysed, mainly on the base on fractographic interpretation and microstructure identification of weak sites in studied aluminium PM alloys. However, the interpretation of the fracture/microstructure overview of the porosity phenomena as a potential fracture initiation sites is still open, owing to be no direct experimental confirmation of the operation of these processes [26]. Critical to further advances in this topic, will be the systematic study of the influence of important variables such as strain hardening, localized shear, grain boundaries, triple junction, second phases and other.

One of the possibilities for the evaluation of the critical pore size is a mathematical description.

It can be seen that during the ECAP process pores become closed and separated.

A two-stage method, based on local polynomial fitting for a non-linear regression model of porosity behaviour, was used (Eqs. 3 and 4) corresponding to Figs. 4a and 4b, respectively.

$$y = 0.4814 \cdot x^2 - 2.9012 \cdot x + 6.2235 \quad [-] \qquad (3)$$

$$y = 0.0910 \cdot x^2 - 0.7606 \cdot x + 3.4104 \quad [-] \qquad (4)$$

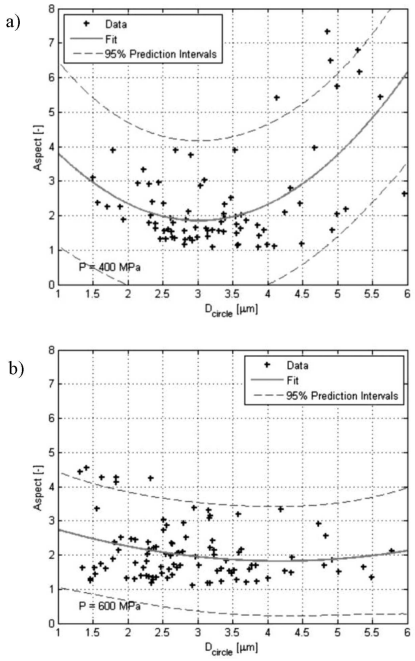

Fig. 4. a) 95% prediction intervals of dependence aspect vs. D_{circle} at 400 MPa pressing pressure, sintering and ECAP; b) 95% prediction intervals of dependence aspect vs. D_{circle} at 600 MPa pressing pressure, sintering and ECAP

It is possible to quantify the pore size dimension representing the critical pore size. It is well-known that the porosity in the sintered materials controls fracture and is responsible for its early onset [32]. As sintered materials generally contain relatively large volume of coarse pores, localised internal necking is able to start at relatively low plastic strains. The large pores lead to high stress concentrations, thus accelerating the spread of fracture.

The basic assumption for the proposed model presented in this paper is that cracks start at the largest pore in the stressed volume; this means that the size of the largest pore must be estimated. Pores, present within the dash line, do not necessarily mean a loss of mechanical properties. Moreover, in specimens processed by ECAP, the mean stress is responsible for the radial growth rate of pores and for equivalent stress, which correlates more closely with changes in pore shape and has a stronger effect on the elliptic pores. The shear component of the applied stress causes particle rearrangement and the collapse of large pores. The particle rearrangement and macroscopic deformation of pores increase the number of particle contacts, meaning a better overall bonding in the component. To investigate the connection between porosity and strength, the size of the largest pore has thus to be modelled in future works. Then, by treating the pore as a sufficiently sharp notch, a fracture mechanics model must be used to link pore size to the strength of the material.

5. Conclusion

The following conclusions may be derived:

1. ECAP decreases the porosity content and the diameter of pores due to severe plastic deformation and also decreases the aspect ratio by the particles alignement.

2. Basing on the mathematical description of porosity, it is possible to quantify when the pore size represents a critical value.

Acknowledgements

This work was financially supported by the projects: VEGA 1/0385/11.

REFERENCES

[1] M.S.T. Weglowski, A. Pietras, Arch. Metall. Mater. **56**, 779 (2011).
[2] P. Bazarnik, M. Lewandowska, K.J. Kurzydlowska, Arch. Metall. Mater. **57**, 869 (2012).
[3] R.K. Islamgaliev, N.F. Yunusova, M.A. Nikitina, K.M. Nesterov, Rev. Adv. Mater. Sci. **25**, 241 (2010).
[4] J.-C. Lee, H.-K. Seok, J.-Y. Suh, Acta Mater. **50**, 4005 (2002).
[5] T. Kvačkaj, A. Kovacova, M. Kvackaj, R. Kocisko, L. Lityńska-Dobrzyńska, V. Stoyka, M. Mihalikova, Micron **43**, 720 (2012).
[6] S. Xu, G. Zhao, X. Ren, Y. Guan, Mater. Sci. Eng. A **476**, 281 (2008).
[7] M. Kvačkaj, T. Kvačkaj, A. Kovacova, R. Kocisko, J. Bacso, Acta Metall. Slovaca **16**, 84 (2010).
[8] T.G. Langdon, Mater. Sci. Forum **519-521**, 45 (2006).
[9] R.Z. Valiev, R.K. Islamgaliev, I.V. Alexandrov, Progr. Mater. Sci. **45**, 103 (2000).

[10] T. Kvačkaj, J. Bidulska, M. Fujda, R. Kočiško, I. Pokorny, O. Milkovič, Mater. Sci. Forum **633-634**, 273 (2010).
[11] M. Matvija, M. Fujda, O. Milkovič, T. Kvačkaj, M. Vojtko, P. Zubko, R. Kočiško, Acta Metall. Slovaca **18**, 4 (2012).
[12] K. Matsuki, T. Aida, T. Takeuchi, J. Kusui, K. Yokoe, Acta Mater. **48**, 2625 (2000).
[13] V.V. Stolyarova, R. Lapovok, I.G. Brodovac, P.F. Thomson, Mater. Sci. Eng. A **357**, 159 (2003).
[14] H. Paul, T. Baudin, F. Brisset, Arch. Metall. Mater. **56**, 245 (2011).
[15] M. Balog, F. Simancik, O. Bajana, G. Requena, Mater. Sci. Eng. A **504**, 1 (2009).
[16] W. Xu, X. Wu, T. Honma, S.P. Ringer, K. Xia, Acta Mater. **57**, 4321 (2009).
[17] M. Chmielewski, J. Dutkiewicz, D. Kalinski, L. Lityńska-Dobrzyńska, K. Pietrzak, A. Strojny-Nedza, Arch. Metall. Mater. **57**, 687 (2012).
[18] S. Rusz, S. Tylšar, J. Kedroň, J. Dutkiewicz, T. Donič, Acta Metall. Slovaca **16**, 229 (2010).
[19] A. Kovacova, T. Kvackaj, M. Kvackaj, I. Pokorny, J. Bidulska, J. Tiza, M. Martikan, Acta Metall. Slovaca **16**, 91 (2010).
[20] E.A. El-Danaf, Mater. Des. **32**, 3838 (2011).
[21] R. Lapovok, J. Mater. Sci. **40**, 341 (2005).
[22] R. Lapovok, D. Tomus, B.C. Muddle, Mater. Sci. Eng. A **490**, 171 (2008).
[23] N.Q. Chinh, J. Gubicza, T. Czeppe, J. Lendvai, Ch. Xu, R.Z. Valiev, T.G. Langdon, Mater. Sci. Eng. A **516**, 248 (2009).
[24] J. Bidulská, R. Kočiško, R. Bidulský, M. Actis Grande, T. Donič, M. Martikán, Acta Metall. Slovaca **16**, 4 (2010).
[25] J. Bidulská, R. Bidulský, M. Actis Grande, High. Temp. Mater. Process. **28**, 337 (2009).
[26] J. Bidulská, T. Kvačkaj, R. Bidulský, M. Actis Grande, Acta Phys.Pol. A **122**, 553 (2012).
[27] J. Bidulská, T. Kvačkaj, R. Kočiško, R. Bidulský, M. Actis Grande, Mater. Sci. Forum **667-669**, 535 (2011).
[28] J. Bidulská, T. Kvačkaj, R. Bidulský, M. Actis Grande, L. Lityńska-Dobrzyńska, J. Dutkiewicz, Chem. Listy **105**, s471 (2011).
[29] J. Bidulská, R. Kočiško, T. Kvačkaj, R. Bidulský, M. Actis Grande, Chem. Listy **105**, s155 (2011).
[30] Nanostructured Materials: Processing, Properties and Potential Applications, ed. C.C. Koch, Noyes Publications, NY 2002, ISBN: 0-8155-1451-4.
[31] J. Bidulská, R. Bidulský, T. Kvačkaj, M. Actis Grande, Steel Res. Int. **83**, 947 (SI), (2012).
[32] G.S. Upadhyaya, Powder Metallurgy Technology, CISP, Cambridge, 2002, ISBN 1898326401.

Received: 20 January 2013.